Obstructed diffusion propagator analysis for single-particle tracking

Aubrey V. Weigel,[1] Shankarachary Ragi,[2] Michael L. Reid,[1] Edwin K. P. Chong,[2,3] Michael M. Tamkun,[4] and Diego Krapf[1,2]
[1]*School of Biomedical Engineering, Colorado State University, Fort Collins, Colorado 80523, USA*
[2]*Department of Electrical and Computer Engineering, Colorado State University, Fort Collins, Colorado 80523, USA*
[3]*Department of Mathematics, Colorado State University, Fort Collins, Colorado 80523, USA*
[4]*Department of Biomedical Sciences and Department of Biochemistry and Molecular Biology, Colorado State University, Fort Collins, Colorado 80523, USA*
(Received 30 December 2011; published 30 April 2012)

We describe a method for the analysis of the distribution of displacements, i.e., the propagators, of single-particle tracking measurements for the case of obstructed subdiffusion in two-dimensional membranes. The propagator for the percolation cluster is compared with a two-component mobility model against Monte Carlo simulations. To account for diffusion in the presence of obstacle concentrations below the percolation threshold, a propagator that includes the transient motion in finite percolation clusters and hopping between obstacle-induced compartments is derived. Finally, these models are shown to be effective in the analysis of Kv2.1 channel diffusive measurements in the membrane of living mammalian cells.

DOI: 10.1103/PhysRevE.85.041924 PACS number(s): 87.15.Vv, 05.40.Fb, 87.14.ep

I. INTRODUCTION

Membrane proteins exhibit complex dynamics, often accompanied by anomalous diffusion. The complexity in protein motion lies in the fact that the plasma membrane is a heterogeneous environment that exhibits microdomain organization, is densely packed with proteins, and is tethered to the cytoskeleton through different proteins and lipids [1]. The diffusion of membrane molecules is studied by a variety of methods that include fluorescence recovery after photobleaching [2], fluorescence correlation spectroscopy [3–5], and single-particle tracking (SPT) [6–8]. In particular, SPT enables the localization of an individual molecule with nanometer precision in real time, yielding detailed information on its molecular motion and the interactions between a protein or lipid with its environment. The diffusive transport of membrane proteins has vital biological implications related to many cellular processes. However, the analysis of anomalous diffusion in live cells is challenging because it can originate via different mechanisms: (a) Membrane proteins and lipids tethered to the cytoskeleton behave as immobile obstacles, hindering the free diffusive transport [9–17]. The resulting motion is termed obstructed diffusion. (b) Macromolecular crowding has been experimentally shown to induce anomalous subdiffusion in some systems [18–20], but the link between anomalous diffusion and crowding is still controversial [21]. It was proposed that crowding gives rise to viscoelastic effects leading to long-time correlations in a particle trajectory [22,23], which may be modeled by fractional Brownian motion (FBM) [24,25]. Nevertheless, the physical mechanism by which crowding can be modeled by FBM is not fully understood. (c) Transient immobilization achieved by temporary binding with a heavy tailed distribution of waiting times lead to subdiffusion and ergodicity breaking [26–28]. This process is modeled by a continuous time random walk (CTRW) [29]. In general, more than one single physical mechanism may be simultaneously responsible for anomalous diffusion in living cells. Recently, we demonstrated that the subdiffusion of Kv2.1 potassium channels in the plasma membrane of mammalian cells is best characterized as a CTRW coexisting with a fractional ergodic mechanism such as obstructed diffusion or FBM [30]. Interestingly, the dynamics of lipid granules in the cytoplasm of yeast have also recently been shown to be influenced by similar mechanisms [31].

Even though obstructed diffusion is not the sole cause for anomalous diffusion in the plasma membrane, it has long been recognized to be an important factor in the diffusion pattern of proteins and lipids. Comparison of diffusion in the axon initial segment (AIS) and blebs shows the relevance of obstruction. *AIS*: An unusually high local density of ankyrin-G and actin forms a region with a large number of immobile obstacles. This obstruction pattern hinders diffusion to such a point that long-range motion is not observed and it effectively functions as a diffusion barrier, a phenomenon that is vital to neuronal polarization [32]. *Blebs*: These spherical protrusions that occur at the periphery of eukaryotic cells [33] lack cytoskeletal anchoring points and are, thus, practically free from immobile obstacles. The diffusion coefficient of proteins in blebs is observed to be dramatically higher than in the rest of the membrane linking the diffusion pattern to cytoskeleton-bound molecules [34].

Several reports show via the use of actin depolymerization drugs that the cytoskeleton is implicated in restricting the diffusion of membrane proteins [10,35]. Truncation of the cytoplasmic domain of membrane proteins was also shown to increase the diffusion coefficient [9,36]. Recently, Andrews *et al*. provided evidence that actin forms a dynamic meshwork involved in forming barriers to free diffusion [12]. In contrast, the ectodomain of some proteins is the key determinant of their lateral diffusion suggesting that anomalous subdiffusion in the plasma membrane can be also induced by interactions with the extracellular matrix or the ectodomains of neighboring membrane proteins [36]. Kusumi's lab has shown that lipids and proteins in the plasma membrane appear to be temporarily confined to microdomains 30–800 nm in size. Temporal confinement seems to be widespread and it was observed in many different cell types including Chinese hamster ovary, mouse hepatoma, rat kangaroo, fetal rat skin keratinocyte, human embryonic kidney (HEK), HeLa, T24, and normal rat kidney cells [11]. Edidin and co-workers showed that vesicle

trafficking to and from the plasma membrane in combination with barriers to lateral diffusion can maintain microdomains in the cell surface with characteristic lifetimes in the tens of seconds [37,38]. These observations can be explained by the existence of clusters of immobile proteins that behave as discontinued fences in the plasma membrane. In order for a walker to hop between compartments it needs to find a gap in the fence. Alternatively, this is achieved by fluctuations in the position of quasi-immobile obstacles. This mechanism has been referred to as the anchored-protein picket model [10]. Obstructions to diffusion in the cell membrane were also observed with optical tweezers. It was shown that as a molecule is dragged along the plasma membrane it encounters frequent obstacles in its path [39,40]. Both elastic and inelastic barriers were found to be present in the cell membrane with the elastic ones being actin-cytoskeleton dependent [41].

In SPT analysis, the mean square displacement (MSD) measures the apparent diffusion coefficient and provides the simplest type of classification of the diffusion pattern. Brownian motion yields a linear MSD, $\langle r^2(t)\rangle = 2dDt$ where D is the diffusion coefficient and d is the substrate dimension ($d = 2$ for a membrane). In contrast, anomalous subdiffusion is characterized by a sublinear MSD, $\langle r^2(t)\rangle \sim t^{\alpha}$, with $\alpha < 1$ being the subdiffusive exponent [8]. When $\alpha > 1$, the motion is termed superdiffusion. Experimental observations of anomalous diffusion with values of α between 0.1 and 0.9 have been reported by different groups [6,42,43]. Unfortunately, the information obtained from MSD analysis is very limited and, in practice, many anomalous subdiffusion models yield the same MSD power law. The problem is that the MSD analysis does not take advantage of the full probability of displacements $P(r,t)$, viz., the propagator, which is naturally available in SPT measurements [44]. $P(r,t)dV$ gives the probability that a particle at the origin at time zero is found in an element of volume dV at r, at time t. The distribution of displacements for Brownian motion is Gaussian,

$$P(r,t) = \frac{1}{4\pi Dt} e^{-r^2/4Dt}. \tag{1}$$

In order to take advantage of the probability of displacements analysis, without the need to impose bin sizes, the cumulative distribution function (CDF) is used [14,28,44,45]. The CDF $F(r^2,t)$ can be interpreted as the probability that a particle at the origin at time zero is found within a circle of radius r at time t. In a two-dimensional (2D) space, $dV = 2\pi r\, dr$, and thus, $F(r^2,t) = 2\pi \int_0^r P(r',t) r'\, dr'$. This yields a monoexponential function, $F(r^2,t) = 1 - e^{-r^2/4Dt}$, for Brownian motion. A two-component mobility model is often used to distinguish between normal and anomalous diffusion by comparing the residuals from a monoexponential CDF fit and a biexponential fit [11,14,30,46–48]. The two-component cumulative distribution becomes

$$F(r^2,t) = 1 - we^{-r^2/\sigma_1^2} - (1-w)e^{-r^2/\sigma_2^2}, \tag{2}$$

where σ_1^2 and σ_2^2 are the slow- and fast-mobility mean square displacements, respectively, i.e., $\sigma_i^2 = 4D_i t$, with weighting factor w.

The propagators for a CTRW and FBM are well documented. The particle displacement of a CTRW is given by a Fox function [49–52] and that of FBM is a Gaussian distribution with a time-dependent diffusion coefficient [53]. However there is a great deal of confusion in the literature about the propagators for obstructed diffusion. Obstructed diffusion can be modeled as a percolation problem. Under the influence of constant thermal agitation, the motion of randomly wandering molecules is closely related to a random walk. Monte Carlo calculations are particularly suitable to simulate the effect of obstruction in the cell membrane because a random set of lattice sites can be directly blocked. Diffusion in a percolation cluster has been extensively studied near criticality [54,55] and, in a series of seminal papers, Saxton has simulated diffusion in the presence of both mobile and immobile obstacles with a wide range of obstacle concentrations, elucidating many of the obstructed diffusion and crowding theoretical predictions [15,56]. The work presented here builds on these reports.

In this study, we report Monte Carlo simulations to characterize the motion of particles in the presence of immobile objects. We describe a method to analyze the particle trajectory based on the distribution of displacements taking into consideration the fractal dimension of the matrix and the fractal dimension of the walk. The dimension of the walk is found from the simulated trajectory. The dimension of the matrix describes the fractal on which the tracer performs a random walk. This matrix is naturally embedded in a 2D space. Because of the self-similarity properties of percolation clusters, obstructed diffusion bears a vast resemblance to FBM. We apply a recently developed method based on p variation [57] to evaluate the underlying mechanism of anomalous diffusion and show that both FBM and obstructed diffusion give the same results. Finally, we compare simulation results to recently reported single-particle tracking measurements of Kv2.1 potassium channels in the membrane of living cells [30].

II. MATERIALS AND METHODS

A. Obstructed diffusion simulations

We implemented random walk simulations on a 2D square lattice to model obstructed diffusion. Obstacles were randomly distributed on the lattice at a concentration c. Obstructed diffusion simulations were implemented in MATLAB using a "blind ant" algorithm. First, we generated a lattice where each site was assigned a random number between 0 and 1. All sites with a number smaller than c are considered obstacles. A walker is placed in the center of the lattice and it is only allowed to move into vacancies, which are sites with assigned numbers bigger than c. The walker attempts to move to one of the four nearest-neighbor sites with equal probability. If the chosen site is blocked, the walker remains at the original position. The clock ticks independent of the outcome of the attempted jump and the protocol is looped N times. The MATLAB built-in algorithm used for random number generation is based on the Mersenne twister algorithm [58]. The results returned are pseudorandom values drawn from a standard uniform distribution.

All lattice generated were 2000 × 2000 sites and periodic boundary conditions were implemented on the random walks. We created three different lattices for each obstacle concentration and obtained three random walks of 2×10^6 steps,

per lattice. Each of these nine random walks was then fit independently according to the text. All results presented here show the mean ± standard deviation of the distribution of fitting results.

B. Single-particle tracking in living cells

We have recently reported single-particle tracking measurements of Kv2.1 potassium channels in live cells [30]. In brief, HEK293 cells were transfected with Kv2.1 channels containing an extracellular biotin acceptor domain that is the substrate for BirA biotin ligase. The transfected cells were incubated with streptavidin-conjugated quantum dots (Qdot 655, Invitrogen, Carlsbad, CA), which bound to the biotinylated Kv2.1 channels. Quantum dots enabled us to track individual channels with nanometer accuracy. The basal membrane of the labeled cells was imaged using a home-built objective-type total internal reflection fluorescence microscope. Quantum dots were excited with a 473 nm laser line and the fluorescence was collected in a back-illuminated electron-multiplied charge coupled device camera (Andor iXon DU-888). Both the stage (Bioptechs, Butler, PA) and the objective were maintained at 37 °C. Individual particles were localized and tracked by fitting the intensity image of an appropriate region of interest to a two-dimensional Gaussian function [30,59].

III. RESULTS

A. Diffusion in an infinite percolation cluster

When the concentration of obstacles is low, small clusters of connected occupied sites, i.e., fences, are formed. Below a critical concentration threshold, the cluster size remains finite but as the concentration increases, so does the mean cluster size. At criticality, an infinite cluster of obstacles develops and the system undergoes a percolation transition. Havlin *et al.* [55,60] have shown that the propagator for an infinite percolation cluster can be described by $P(r,t) \sim r^{d_f-d} f(r/t^{1/d_w})$, where d_w is the fractal dimension of the walk, d_f is the fractal dimension of the cluster, d is the underlying dimension, and $f(u) = \exp(-K_0 u^{1.65})$. A percolation cluster in a membrane is characterized by a fractal dimension $d_f = 1.896$, $d = 2$, and the subdiffusive exponent is given by d_w: $MSD \sim t^{2/d_w}$. In a percolation cluster, the propagator gives the probability density that a particle is found in an element of volume dV within a random fractal with dimension d_f, given by [61]

$$dV = \frac{2\pi^{d_f/2}}{\Gamma(d_f/2)} r^{d_f-1}\, dr, \tag{3}$$

where gamma is the Gamma function, $\Gamma(x) = \int_0^\infty e^{-t} t^{x-1}\, dt$. Equation (3) yields

$$P(r,t) = B r^{d_f-d} \exp[-K(t) r^{1.65}], \tag{4}$$

$$B = \frac{1.65\Gamma(d_f/2)}{2\pi^{d_f/2}\Gamma[(2d_f-d)/1.65]} K(t)^{(2d_f-d)/1.65}, \tag{5}$$

where $K(t) = a/t^{1.65/d_w}$, $d_f - d = -0.104$, and B is the normalization factor. Integrating over the fractal volume, the cumulative distribution is

$$F(r^2,t) = \frac{\gamma[(2d_f-d)/1.65, K(t) r^{1.65}]}{\Gamma[(2d_f-d)/1.65]}, \tag{6}$$

where $\gamma(a,x)$ is the incomplete gamma function defined by $\gamma(a,x) = \int_0^x e^{-t} t^{a-1}\, dt$. Because d_f and d are known, the CDF is defined by a single parameter $K(t)$.

The critical obstacle concentration threshold in a square lattice is 40.7255 ± 0.0002% [62]. Figure 1(a) shows a CDF of a simulated trajectory for a walker in a square lattice at criticality. The fit to the percolation model [Eq. (6)] is shown together with the fits to simple diffusion (Gaussian propagator) and to a two-component mobility model [Eq. (2)]. While both simple diffusion and an infinite percolation cluster model are characterized by a single parameter, the two-component mobility model is fit to three parameters. Both the two-component and the percolation cluster fits are of good quality, with the two-component model being slightly better. As discussed below, the percolation cluster fitting parameter reproduces well the predicted power law $K(t) = a/t^{1.65/d_w}$, with $d_w = 2.8$. The same value is found from the MSD subdiffusive exponent.

The cumulative distribution eliminates the dependence on bin size and it integrates out noise but the displacement probability is more informative from a qualitative perspective. In order to compute the displacement distribution $P(r,t)$, the number of displacements, i.e., root of square displacements, between $r - \Delta r/2$ and $r + \Delta r/2$ is counted and the occurrences are normalized by the bin volume, $\Delta V = 2\pi r \Delta r$. However, this procedure introduces a large degree of error at small r values. This method also assumes a 2D underlying space, which is incorrect for diffusion on a fractal structure. A more suitable procedure involves computing the number of displacements and renormalizing the propagator in order to show $P(r,t)\Delta V$. Figure 1(b) shows the propagators using the results from the CDF fits. For diffusion in a percolation cluster, the normalization volume, as given by Eq. (3), is $\Delta V_{d_f} = 2\pi^{d_f/2} r^{d_f-1} \Delta r / \Gamma(d_f/2)$. Figure 1(c) shows the distribution of displacements normalized to a 2D space. The comparison shows that the raw-displacement occurrences [as shown in Fig. 1(b)] provide better visual results.

B. Diffusion in a deterministic fractal

The percolation cluster at criticality can be described by a random fractal with dimension d_f. Thus, it is interesting to compare this motion with the propagator for diffusion in a deterministic fractal, which was derived by O'Shaugnessy and Procaccia [63],

$$P(r,t) = \frac{d_w \Gamma(d_f/2)}{2\pi^{d_f/2}\Gamma(d_f/d_w)} \left(\frac{1}{4D_F t}\right)^{d_f/d_w} \exp\left(-\frac{r^{d_w}}{4D_F t}\right). \tag{7}$$

Integrating over the fractal volume [14] given by Eq. (2) yields

$$F(r^2,t) = \gamma(d_f/d_w, r^{d_w}/4D_F t)/\Gamma(d_f/d_w), \tag{8}$$

which includes three independent parameters, d_f, d_w, and D_F, that are constrained by the fractal structure: $1 < d_f \leqslant 2$

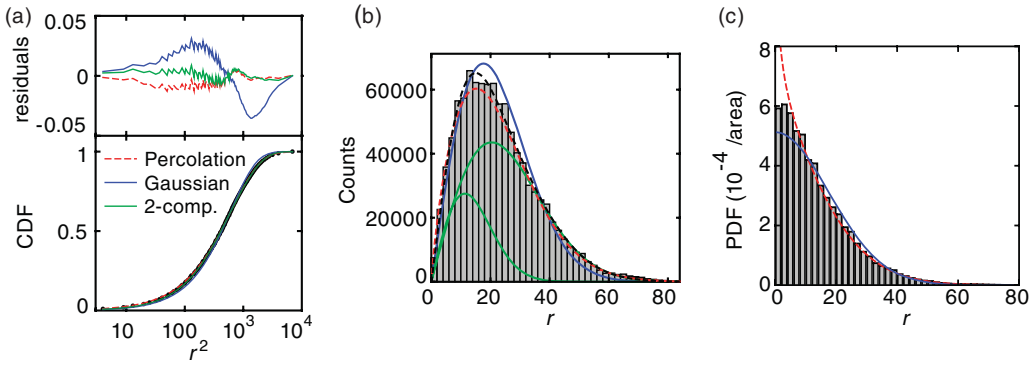

FIG. 1. (Color online) Propagator analysis of diffusion of a representative trajectory in a percolation cluster close to criticality. The data were generated from the random walk simulations on a square lattice with an obstacle concentration of 41%, i.e., $c/c_P = 1.007$. (a) CDF at $t = 10\,000$ with fits to percolation cluster as a dashed red line [Eq. (6)], normal diffusion as a solid blue line (Gaussian), and two-component mobility as a green line [light gray, Eq. (2)]. (b) Histogram of displacements. The continuous lines show the renormalized propagators $P(r,t)\Delta V$, obtained from the fit to the CDF. Each Gaussian of the two-component mobility model is shown as a green line (light gray) independently for clarity and the sum of the two components is shown as a black dashed line. (c) Probability density function obtained by normalizing the distribution of displacements for $t = 10\,000$. The distribution is normalized by the volume $\Delta V_{2D} = 2\pi r \Delta r$, where Δr is the bin size. The propagators of percolationlike and normal diffusion, as obtained from the fits to the CDF, are shown. Because the propagator of diffusion in a percolation cluster operates in d_f dimensions, the curve shown is $P(r,t)\Delta V_{d_f}/\Delta V_{2D}$, where ΔV_{d_f} is the volume corresponding to a fractal dimension d_f, as in the text.

and $d_w \geqslant 2$. This model has been successfully applied to obstructed diffusion experimental measurements in supported lipid bilayers [14]. We have modeled our simulations using this equation and found a best nonlinear fit when $d_w = 2.05 \pm 0.05$. This value disagrees with the value found from the MSD subdiffusive exponent ($d_w = 2.8$). For comparison, the residuals for the deterministic fractal model with $d_w = 2$ and $d_w = 2.8$ are shown together with the two-component model in Fig. 2(a). Fitting Eq. (8) to the CDF of our simulation also yields a time-dependent coefficient D_F [Fig. 2(b)], which is not consistent with a deterministic fractal, indicating the failure of this model to describe obstructed diffusion.

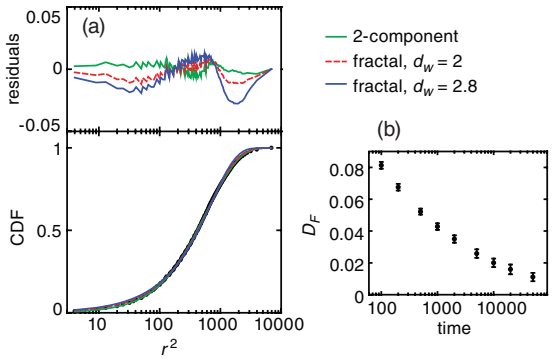

FIG. 2. (Color online) CDF of simulated obstructed diffusion with obstacle concentration $c = 0.41$ at lag time $t = 10\,000$. (a) The CDF of a representative trajectory is modeled by a deterministic fractal as given by Eq. (6). The best nonlinear fit is found for $d_w = 2$ and $d_f = 1.6$ (dashed red line). Note that the fit is constrained by $d_w \geqslant 2$. For comparison the biexponential fit [Eq. (2)] and the fit using $d_w = 2.8$ are also shown. (b) The diffusion coefficient D_F is shown as found from fitting to the CDF at different lag times to a deterministic fractal model [Eq. (8)]. All the CDFs are described by $d_w = 2$.

C. Obstructed diffusion below the percolation threshold

For the analysis of obstructed diffusion in cellular environments, it is necessary to consider a wider obstacle concentration range than that close to the percolation threshold. At criticality, an infinite percolation cluster is formed and diffusion is anomalous on all time scales [54]. At concentrations below the percolation threshold, Saxton [15] has shown that diffusion is anomalous at short times and becomes normal at long times. The crossover time increases as the concentration of obstacles approaches the threshold. The transition from anomalous to normal diffusion can be observed in plots of $\log[\langle r^2\rangle/t]$ as a function of $\log t$. Normal diffusion yields a constant, while subdiffusion yields a power law with an exponent $(2/d_w) - 1$ [15]. This can be observed for concentrations below and at the percolation threshold in Fig. 3. It has been shown [15] that when the data are presented as a function of c/c_P, where c is the obstacle concentration and c_P is the percolation threshold, the results do not depend on the lattice geometry or obstacle size. For comparison of obstructed diffusion with fractional Brownian motion, we have applied a p-variation test (see Supplemental Material and Fig. S1 [64]) on our simulations [57]. However, the obstructed diffusion and fractional Brownian motion cannot be distinguished within this test.

We have tested the percolation model on our simulations. The main result obtained from the percolation propagator is the parameter $K(t)$ from Eqs. (4) and (6). Results are presented as a function of lag time in Fig. 4. $K(t)$ clearly follows a power law $K(t) = a/t^{1.65/d_w}$. Note that while d_w depends on the cluster size, d_f is universal [54] thus d_w is the only parameter that varies with obstacle concentration. To obtain a single scalar statistic for the goodness of fit, it is reasonable to use an aggregate or mean squared residual. This statistic is common in several standard goodness-of-fit tests, including the chi-square [65] and Cramér–von Mises [66]

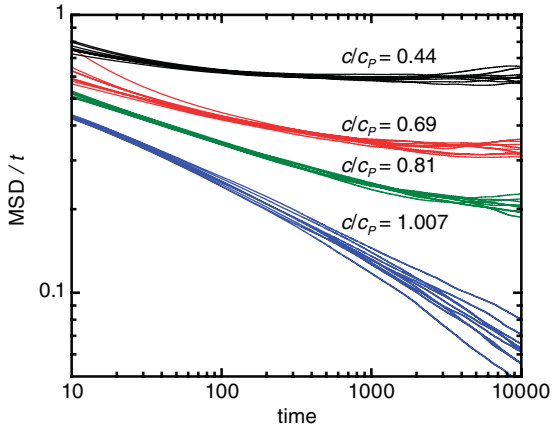

FIG. 3. (Color online) $\langle r^2\rangle/t$ as a function of t in a log-log scale for a tracer in the presence of immobile obstacles at different concentrations. $\langle r^2\rangle$ is the mean square displacement and t is the lag time. All nine simulated trajectories are shown together for each obstacle concentration.

tests. Comparing the mean squared errors of the percolation model to that of the two-component mobility fit (Fig. 5), it is observed that at concentrations close to the percolation threshold, both models give similar results. However, for lower obstacle concentrations, the results from the two-component mobility are significantly better.

The slope of $\log[K(t)]$ vs $\log(t)$ in Fig. 4 is $-1.65/d_w$, thus, by means of the percolation cluster model, the fractal dimension of the walk d_w is obtained for each obstacle concentration. Figure 6 shows d_w obtained in this manner for a wide range of obstacle concentrations. It is seen that d_w increases smoothly from 2 to 2.8, reaching this value when the obstacle concentration equals the percolation threshold, i.e., $c = c_P$. This result is not surprising and it is the same that is obtained by fitting the MSD [15]. However, when the form of the propagator is known, fitting the propagator bears the advantage that the whole distribution of displacements is used instead of only the second moment. Because the whole distribution is used and the fit has a single unknown parameter, the accuracy of the obtained d_w values is fairly high as seen by

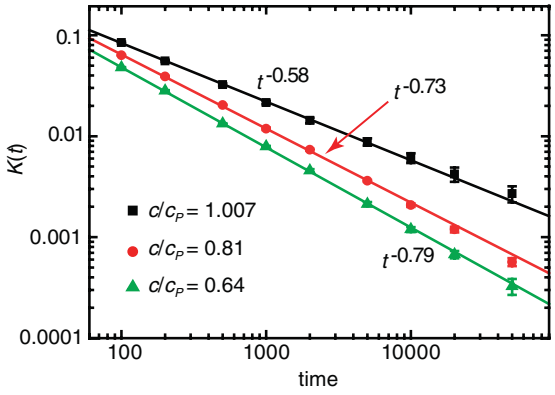

FIG. 4. (Color online) Percolation fit parameter $K(t)$ in Eq. (6) as a function of lag time at two moderate obstacle concentrations and close to criticality. The parameter exhibits a power law $K(t) = a/t^{1.65/d_w}$.

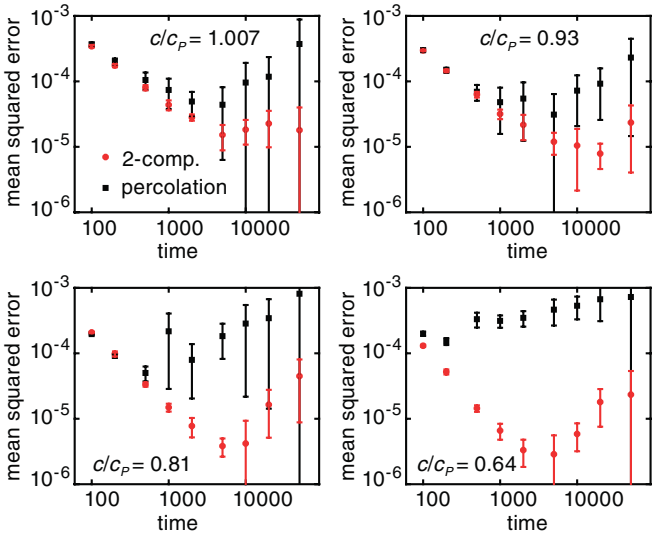

FIG. 5. (Color online) Mean squared errors of the fits to the obstructed diffusion simulations with different obstacle concentrations using the two-component mobility and the percolation cluster models.

the small error in d_w at each concentration. This reduces the need for averaging over many trajectories and also allows the study of shorter paths.

As expected, the MSD of the fast mobility in the two-component mobility model follows a similar trend as the percolation model with $\sigma_2^2 \sim t^{2/d_w}$. Results of ${\sigma_i}^2$ versus lag time are presented in Fig. 7(a) showing that σ_2^2 follows a power law. The time dependence of σ_2^2 yields $2/d_w$ [shown in Fig. 7(b)]. At concentrations close to criticality this empirical model gives robust results but it becomes very unreliable for lower concentrations. Thus for lower concentrations the error bars in $2/d_w$ cover a large range from subdiffusion to superdiffusion, rendering this model useless unless a very large amount of data is available.

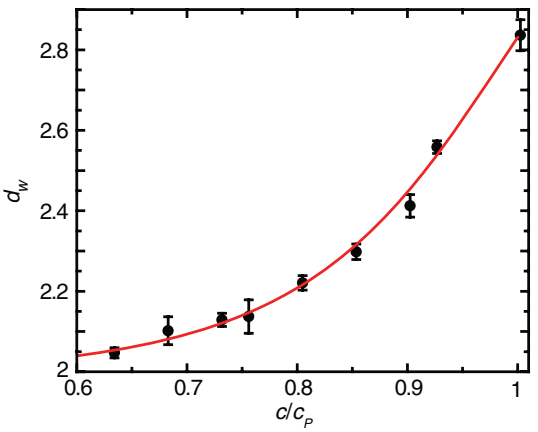

FIG. 6. (Color online) Fractal dimension of the walk d_w as a function of relative obstacle concentration. d_w is obtained from the fit to the percolation model as shown in Fig. 4. The red line is a least square fit to d_w as performed in Ref. [15]: $d_w = (2 - 3.630x + 1.758x^2)/(1 - 1.806x + 0.850x^2)$, where $x = c/c_P$, c is the obstacle concentration, and c_P is the concentration at criticality.

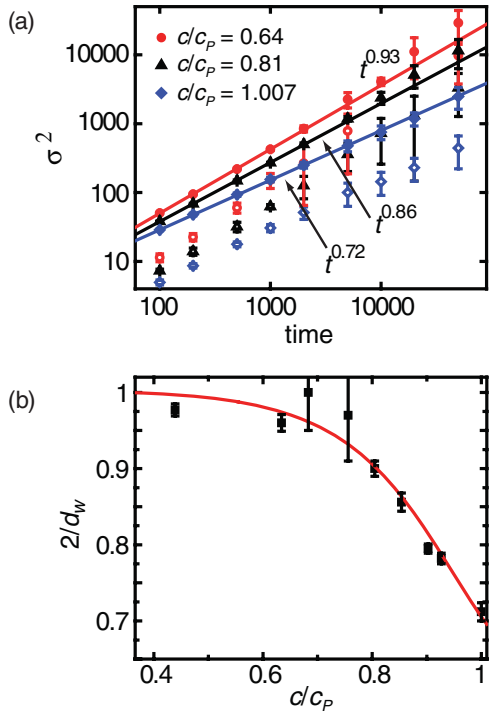

FIG. 7. (Color online) Two-component mobility model. (a) MSD of each of the two mobilities. Full symbols: fast component. Hollow symbols: slow component. (b) Subdiffusion exponent as a function of relative obstacle concentration. The red line is the function found from the least square fit in Fig. 6.

D. Derivation of a propagator for obstructed diffusion below the percolation threshold

The exact propagator of this problem combines percolationlike diffusion at short distances and normal diffusion at long distances. The difficulty in this model is that the two parts operate on different dimensions. Percolationlike short-distance diffusion acts on d_f dimensions but long-range normal diffusion is performed in two dimensions. Thus, we cannot integrate this function in a straightforward way because both parts have different Jacobians, i.e., different differential volumes. If we allow a percolation part $P_1 dV_1$ according to Eqs. (3) and (4), and a normal diffusion part $P_2 dV_2$ according to Eq. (1), we obtain $P(r,t)dV = \omega P_1\, dV_1 + (1-\omega)P_2\, dV_2$. Then,

$$P(r,t)dV = \left[\frac{1.65\omega}{\Gamma\left(\frac{2d_f-d}{1.65}\right)} K(t)^{(2d_f-d)/1.65} r^{2d_f-d-1} \times \exp\left(-K(t)r^{1.65}\right) + (1-\omega)\frac{2r}{\sigma_1^2}\exp\left(-\frac{r^2}{\sigma_1^2}\right)\right]dr, \tag{9}$$

where ω, $K(t)$, and σ_1 are defined previously. All three parameters are time dependent. The cumulative distribution function is

$$F(r^2,t) = \omega\frac{\gamma[(2d_f-d)/1.65, K(t)r^{1.65}]}{\Gamma[(2d_f-d)/1.65]} + (1-\omega)\left(1-e^{-r^2/\sigma_1^2}\right). \tag{10}$$

These equations give the accurate distribution of displacements for obstructed diffusion with any obstacle concentration below the percolation threshold. However, as in the two-mobility model they involve three different fitting parameters, which means that more data is needed to fit this function than the simple percolation approximation.

E. Comparison to experimental data

It is possible to use the percolation model to obtain information on the obstacle concentration for diffusion in an obstructed environment. Kv2.1 potassium channels are best modeled by a nonergodic CTRW on a percolation cluster [30]. However, when cells are treated with actin polymerization inhibitors, such as swinholide A, the CTRW is eliminated and ergodicity is recovered. After treatment with swinholide A, the diffusion is still anomalous over lag times of more than two decades [Fig. 8(a)]. We have previously proposed [30] that the reason for this anomaly is the presence of immobile obstacles in the plasma membrane which obstruct the path of the Kv2.1 channels. While in three dimensions a particle easily finds a path to escape from obstacle-induced compartments, in 2D the confinement within finite percolationlike compartments is enhanced because there are fewer escape paths [67].

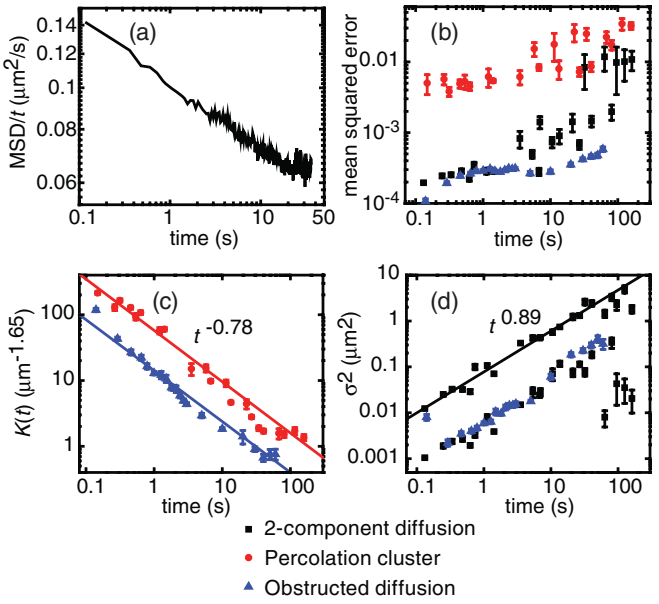

FIG. 8. (Color online) Analysis of experimental Kv2.1 single-particle tracking in the plasma membrane of living HEK cells. All error bars indicate standard error of the mean. (a) $\langle r^2\rangle/t$ as a function of t in a log-log scale. A negative slope between 0.1 and 20 s is evident indicating anomalous subdiffusion across this time scale. (b) Mean squared errors from fitting the CDF at different lag times to three different models as described in the text: two-component mobility, percolation cluster, and obstructed diffusion. (c) $K(t)$ values as a function of t, obtained from fitting the experimental data to the percolation cluster and obstructed diffusion. A power law dependence is obtained from which d_w is found. (d) Mean square displacements obtained by modeling the experimental data with two-component mobility [σ_1^2 and σ_2^2 in Eq. (2)], and with obstructed diffusion [σ_1^2 in Eq. (10)]. The slow-mobility component MSDs from the two different models coincide.

Figure 8(b) shows the mean squared errors obtained from fitting the CDF of Kv2.1 channels in cells treated with swinholide A to a percolation cluster [Eq. (6)], to a two-component mobility model [Eq. (2)], and to the subcritical obstructed diffusion propagator derived in Eq. (10). The obstructed diffusion propagator gives the smallest mean squared errors over all lag times. These results correspond to the mean from 158 trajectories. A mixed propagator result is shown in Fig. S2 together with the plots for $\omega = 0$ and $\omega = 1$ [64]. The percolation cluster and the obstructed diffusion models yield values of $K(t)$ that scale as a power law in the same fashion as the obstructed diffusion simulations [Fig. 8(c)]. From these fits, the fractal dimension of the walk is obtained, $d_w = 2.12 \pm 0.08$. It is also observed in Fig. 8(c) that both models yield very similar values for d_w. Using the empirical fit in Fig. 6, $d_w = (2 - 3.630x + 1.758x^2)/(1 - 1.806x + 0.850x^2)$, where $x = c/c_P$, we can calculate the relative obstacle concentration. A range between 0.62 and 0.79 is obtained for c/c_P. Figure 8(d) shows the results of the fast- and slow-mobility MSDs from the two-component model and the slow-mobility (long-range) MSD from the obstructed diffusion model. The long-range MSDs for the two models match satisfactorily but the values obtained with the obstructed diffusion propagator are less prone to errors, particularly at large lag times.

IV. DISCUSSION

Analysis of the CDF at different lag times provides important information. The simulations presented here show that, independent of the obstacle concentration, the CDF can be approximated to either a two-component mobility model or a percolation cluster. One could always argue that the two-component mobility model introduces two additional fitting parameters and thus the model fits better to the simulation in the trivial way, regardless of the actual process. However, the two-component model actually approaches the propagator of obstructed diffusion because the obstacles form fences which in turn compartmentalize the cell membrane. Thus, for short distances, the particle moves according to a fast mobility within a single compartment. For long distances, the particle traverses several compartments and it resembles a tracer that diffuses with a slow mobility. The reason this model is not exact is that at short distances the motion is performed within a finite percolation cluster, thus the substrate is a random fractal of dimension d_f, but at long distances the motion is normal according to a substrate with dimension $d = 2$.

The percolation propagator gives excellent results close to the percolation threshold. At small obstacle concentrations, this model fits worse than the two-component mobility. The cause for the deterioration of the fit quality is that the percolation model does not account for the transition to normal diffusion. In spite of this shortcoming, the percolation model can be used to obtain information on the membrane structure without the need for extensive data. We observe that this model is more robust than the two-component model.

The analysis presented here suggests Kv2.1 channels in cells treated with swinholide A undergo anomalous diffusion due to an intermediate concentration of immobile obstacles leading to transient percolationlike motion. The presence of anchored proteins has been proposed by Kusumi and co-workers to be partially responsible for the diffusion anomaly seen in the plasma membrane [68]. Complexity in cell membranes is also enhanced by the presence of fast- and slow-moving obstacles. Experimental evidence shows that the diffusion of streptavidin in solutions crowded with bovine serum albumin (BSA) is anomalous [18]. Diffusion of proteins in solutions of random-coil polymers at high concentrations is significantly more anomalous than in BSA solutions [18,19]. It was proposed that subdiffusion induced by rapidly moving obstacles may be grounded in a FBM process [19]. Whether anomalous diffusion in the nucleus and cytoplasm is percolationlike or FBM is still under debate [69]. Scaling similarities between the two models further complicates the discrimination. In the plasma membrane of a living cell, it is likely that both mobile (fast- and slow-moving) and immobile obstacles are present and maybe both FBM and percolation are responsible for the diffusion anomaly. This problem may be addressed in the future by studying supported lipid bilayers under controlled conditions in order to discriminate between these two processes. Equations (9) and (10) derived here provide a good platform for the analysis of the obstructed diffusion component.

V. CONCLUSIONS

In conclusion, we have provided a method for the analysis of propagators of obstructed subdiffusion in single-particle tracking data. The propagator for the percolation cluster at criticality is explicitly given and is shown against Monte Carlo simulations, in order to eliminate confusion and disagreement commonly found in the literature. We have also derived the propagator for obstructed diffusion at obstacle concentrations below the percolation threshold by combining a percolation model with hop diffusion between obstacle-induced compartments. By analyzing the time dependence of the propagator, it is possible to obtain information on the concentration of immobile obstacles. Experimental data from Kv2.1 channels in live mammalian cells treated with an actin polymerization inhibitor were analyzed using the derived obstructed diffusion propagator. The obstructed diffusion propagator provided good agreement with the experimental data. The discrimination between percolation and fractional Brownian motion is shown to be highly complex, even with the use of advanced tests such as the p-variation method. The propagators of the two models are qualitatively different, but a non-Gaussian propagator as seen here is not enough to exclude the combination of both obstructed diffusion and FBM.

ACKNOWLEDGMENT

This material is based upon work supported by the National Science Foundation under Grant No. 0956714.

[1] D. M. Engelman, Nature (London) **438**, 578 (2005).
[2] D. Axelrod, D. E. Koppel, J. Schlessinger, E. Elson, and W. W. Webb, Biophys. J. **16**, 1055 (1976).
[3] S. Maiti, U. Haupts, and W. W. Webb, Proc. Natl. Acad. Sci. USA **94**, 11753 (1997).
[4] E. Haustein and P. Schwille, Methods **29**, 153 (2003).
[5] O. Krichevsky and G. Bonnet, Rep. Prog. Phys. **65**, 251 (2002).
[6] R. N. Ghosh and W. W. Webb, Biophys. J. **66**, 1301 (1994).
[7] H. Bannai, S. Levi, C. Schweizer, M. Dahan, and A. Triller, Nat. Protoc. **1**, 2628 (2006).
[8] M. J. Saxton and K. Jacobson, Annu. Rev. Biophys. Biomol. Struct. **26**, 373 (1997).
[9] M. Edidin, M. C. Zuniga, and M. P. Sheetz, Proc. Natl. Acad. Sci. USA **91**, 3378 (1994).
[10] T. Fujiwara, K. Ritchie, H. Murakoshi, K. Jacobson, and A. Kusumi, J. Cell Biol. **157**, 1071 (2002).
[11] K. Murase *et al*., Biophys. J. **86**, 4075 (2004).
[12] N. L. Andrews, K. A. Lidke, J. R. Pfeiffer, A. R. Burns, B. S. Wilson, J. M. Oliver, and D. S. Lidke, Nat. Cell Biol. **10**, 955 (2008).
[13] P. H. Lommerse, G. A. Blab, L. Cognet, G. S. Harms, B. E. Snaar-Jagalska, H. P. Spaink, and T. Schmidt, Biophys. J. **86**, 609 (2004).
[14] M. A. Deverall, E. Gindl, E. K. Sinner, H. Besir, J. Ruehe, M. J. Saxton, and C. A. Naumann, Biophys. J. **88**, 1875 (2005).
[15] M. J. Saxton, Biophys. J. **66**, 394 (1994).
[16] B. J. Sung and A. Yethiraj, Phys. Rev. Lett. **96**, 228103 (2006).
[17] M. R. Horton, F. Hofling, J. O. Radler, and T. Franosch, Soft Matter **6**, 2648 (2010).
[18] D. S. Banks and C. Fradin, Biophys. J. **89**, 2960 (2005).
[19] J. Szymanski and M. Weiss, Phys. Rev. Lett. **103**, 038102 (2009).
[20] M. Weiss, M. Elsner, F. Kartberg, and T. Nilsson, Biophys. J. **87**, 3518 (2004).
[21] J. A. Dix and A. S. Verkman, Annu. Rev. Biophys. **37**, 247 (2008).
[22] M. Weiss, G. Guigas, and C. Kalla, Biophys. J. **93**, 316 (2007).
[23] W. C. Pan, L. Filobelo, N. D. Q. Pham, O. Galkin, V. V. Uzunova, and P. G. Vekilov, Phys. Rev. Lett. **102**, 058101 (2009).
[24] B. Mandelbrot and J. W. Van Ness, SIAM Rev. **10**, 422 (1968).
[25] M. J. Saxton, Biophys. J. **81**, 2226 (2001).
[26] T. J. Feder, I. Brust-Mascher, J. P. Slattery, B. Baird, and W. W. Webb, Biophys. J. **70**, 2767 (1996).
[27] M. J. Saxton, Biophys. J. **70**, 1250 (1996).
[28] S. J. Sahl, M. Leutenegger, M. Hilbert, S. W. Hell, and C. Eggeling, Proc. Natl. Acad. Sci. USA **107**, 6829 (2010).
[29] H. Scher and E. W. Montroll, Phys. Rev. B **12**, 2455 (1975).
[30] A. V. Weigel, B. Simon, M. M. Tamkun, and D. Krapf, Proc. Natl. Acad. Sci. USA **108**, 6438 (2011).
[31] J. H. Jeon, V. Tejedor, S. Burov, E. Barkai, C. Selhuber-Unkel, K. Berg-Sorensen, L. Oddershede, and R. Metzler, Phys. Rev. Lett. **106**, 048103 (2011).
[32] C. Nakada, K. Ritchie, Y. Oba, M. Nakamura, Y. Hotta, R. Iino, R. S. Kasai, K. Yamaguchi, T. Fujiwara, and A. Kusumi, Nat. Cell Biol. **5**, 626 (2003).
[33] C. C. Cunningham, J. Cell Biol. **129**, 1589 (1995).
[34] D. W. Tank, E. S. Wu, and W. W. Webb, J. Cell Biol. **92**, 207 (1982).
[35] Y. M. Umemura, M. Vrljic, S. Y. Nishimura, T. K. Fujiwara, K. G. N. Suzuki, and A. Kusumi, Biophys. J. **95**, 435 (2008).
[36] F. Zhang, G. M. Lee, and K. Jacobson, Bioessays **15**, 579 (1993).
[37] L. A. Gheber and M. Edidin, Biophys. J. **77**, 3163 (1999).
[38] Y. Lavi, M. A. Edidin, and L. A. Gheber, Biophys. J. **93**, L35 (2007).
[39] M. Edidin, S. C. Kuo, and M. P. Sheetz, Science **254**, 1379 (1991).
[40] Y. Sako and A. Kusumi, J. Cell. Biol. **129**, 1559 (1995).
[41] K. Suzuki, R. E. Sterba, and M. P. Sheetz, Biophys. J. **79**, 448 (2000).
[42] R. Simson, B. Yang, S. E. Moore, P. Doherty, F. S. Walsh, and K. A. Jacobson, Biophys. J. **74**, 297 (1998).
[43] P. R. Smith, I. E. G. Morrison, K. M. Wilson, N. Fernandez, and R. J. Cherry, Biophys. J. **76**, 3331 (1999).
[44] G. J. Schutz, H. Schindler, and T. Schmidt, Biophys. J. **73**, 1073 (1997).
[45] M. Vrljic, S. Y. Nishimura, S. Brasselet, W. E. Moerner, and H. M. McConnell, Biophys. J. **83**, 2681 (2002).
[46] J. M. Crane and A. S. Verkman, Biophys. J. **94**, 702 (2008).
[47] M. J. M. Schaaf, W. J. A. Koopmans, T. Meckel, J. van Noort, B. E. Snaar-Jagalska, T. S. Schmidt, and H. P. Spaink, Biophys. J. **97**, 1206 (2009).
[48] S. Wieser and G. J. Schutz, Methods **46**, 131 (2008).
[49] W. R. Schneider and W. Wyss, J. Math. Phys. **30**, 134 (1989).
[50] S. Khan, A. M. Reynolds, I. E. G. Morrison, and R. J. Cherry, Phys. Rev. E **71**, 041915 (2005).
[51] A. M. Reynolds, Phys. Lett. A **342**, 439 (2005).
[52] R. Metzler and J. Klafter, Phys. Rep. **339**, 1 (2000).
[53] R. Metzler and J. Klafter, J. Phys. A **37**, R161 (2004).
[54] D. Ben-Avraham and S. Havlin, *Diffusion and Reactions in Fractals and Disordered Systems* (Cambridge University Press, Cambridge, 2000).
[55] S. Havlin, D. Movshovitz, B. Trus, and G. H. Weiss, J. Phys. A **18**, L719 (1985).
[56] M. J. Saxton, Biophys. J. **52**, 989 (1987).
[57] M. Magdziarz, A. Weron, K. Burnecki, and J. Klafter, Phys. Rev. Lett. **103**, 180602 (2009).
[58] M. Matsumoto and T. Nishimura, ACM Trans. Model. Comput. Simul. **8**, 3 (1998).
[59] M. K. Cheezum, W. F. Walker, and W. H. Guilford, Biophys. J. **81**, 2378 (2001).
[60] S. Havlin and D. Ben-Avraham, Adv. Phys. **36**, 695 (1987).
[61] A. P. Prudnikov, Y. A. Brychkov, and O. I. Marichev, *Integrals and Series* (Gordon and Breach Science, Amsterdam, 1986), Vol. 1, p. 585.
[62] R. M. Ziff and B. Sapoval, J. Phys. A **19**, L1169 (1986).
[63] B. O'Shaughnessy and I. Procaccia, Phys. Rev. Lett. **54**, 455 (1985).
[64] See Supplemental Material at http://link.aps.org/supplemental/10.1103/PhysRevE.85.041924 for the p-variation test methods, p-variation results, and mixed propagator results.
[65] J. R. Taylor, *An Introduction to Error Analysis: The Study of Uncertainties in Physical Measurements* (University Science Books, Sausalito, CA, 1996), p. 268.
[66] T. W. Anderson, Ann. Math. Stat. **33**, 1148 (1962).
[67] B. J. Sung and A. Yethiraj, J. Phys. Chem. B **112**, 143 (2008).
[68] K. Ritchie, R. Iino, T. Fujiwara, K. Murase, and A. Kusumi, Mol. Membr. Biol. **20**, 13 (2003).
[69] E. Kepten, I. Bronshtein, and Y. Garini, Phys. Rev. E **83**, 041919 (2011).